

# TOWARDS NOISE ABATEMENT FLIGHT PROCEDURE DESIGN:

## DLR Rotorcraft Noise Ground Footprints Model and its Validation

Jianping Yin, Pierre Spiegel, Heino Buchholz

DLR, Institute of Aerodynamics and Flow Technology,  
Technical Acoustics Division,  
Lilienthalplatz 7, 38108 Braunschweig, Germany

### ABSTRACT

As a first step towards noise abatement flight procedure design, this paper presents techniques for rotorcraft noise ground footprint prediction developed/used at DLR, using either purely numerical computations, measured sound fields or measured blade pressures.

The first method adopted for the ground footprint prediction, based on the purely numerical computations consists of a three-step procedure which calculates first the unsteady aerodynamics of the simultaneously turning main- and tail rotor. The aerodynamic code, UPM-Mantic is based on a 3-D unsteady panel method which simulates all motions of an articulated rotor and the relative motion between main- and tail rotor blades. The unsteady pressure distribution on the main- and tail rotor blades serves as input to FW-H equation based code, APSIM to define the acoustic far field pressure on a hemispherical surface beneath the aircraft. The hemispherical sound field in narrow band spectrum together with weather profile, flight trajectory and conditions are provided to a flyover noise prediction code, Hemisphere (re-propagation procedure) to perform footprints prediction. The propagation of the noise on to the ground is treated as "free" propagation with consideration of atmospheric absorption and ground reflection.

The second method of generating acoustic ground footprints consists in using measured acoustic data on limited microphones. The ground to hemisphere transformation, or reverse propagation procedure, embedded in Hemisphere code is first used to transform ground measured acoustic data to a hemisphere surface beneath the rotorcraft. The transformations are performed by correcting back spherical spreading, atmosphere absorbing and ground reflection. In general, the measured data, including weather profile, flight trajectory and

acoustic spectrum are used in the reverse propagation procedure. After obtaining a free field lower hemisphere sound field, the re-propagation procedure in Hemisphere code is then used for a footprint on a user-defined grid of observer locations.

The third method consists in computing the noise, either directly on the ground or on an hemisphere, using measured blade pressures. The Conga code (initially developed at ONERA, using the Paris FW-H equation based code) allows to perform such computations using blade pressure data on few points, especially in BVI conditions.

The comparison of the 3 methods are carried out for a BO105 helicopter, using also measured noise and measured blade pressures of the RONAP flight test conducted on Cochstedt airport, Germany in 2001. The noise ground footprints for the flight conditions, such as 6° descent and 12° takeoff are first simulated using the first method (in a MR and TR configuration, without the fuselage). The two other methods are then used for these flight conditions and for additional descent flight conditions. The methods are compared and cross-check validations are performed. Finally, a simple flight procedure with combination of different segment of flight trajectories is tested to demonstrate the capability of DLR Hemisphere code.

### INTRODUCTION

Helicopter noise source is more complex than fixed-wing aircraft noise because of its highly directional and characteristic impulsive content. The Helicopter flyover noise is varied with flight conditions, such as flight speed and flight path angle. Like fixed-wing aircraft noise, helicopter noise often becomes a source of community annoyance and controversy. Interest in acoustic ground footprints during rotorcraft flight operations

is widening as the commuter traffic increases and the public perception of helicopter noise reaches heightened proportions. This data is also needed by the authorities to assess noise impact on land use planning around suburban and heliport terminal areas. A prediction capability can help to improve rotorcraft noise impact modeling and develop noise abatement procedures for the purpose of noise mitigation.

The most accurate method to generate acoustic footprints is a flight of the aircraft over a large number of ground microphones placed over the area of interest. Since operational aircraft under real flight conditions are employed, a comprehensive picture of the ground footprint is obtained for any flight condition of interest; but the large expense and data acquisition effort needed for this approach severely limit its applicability. The approach, proposed by Wilson et al [1], to generate acoustic ground footprints over a large area, uses acoustic data gathered from only a ground microphone array placed perpendicular to the flight path. Together with aircraft flight dynamics, this data is used to define a hemispherical sound intensity surface beneath the aircraft. The so defined noise source and aircraft tracking data are used as input to NASA /Langley's ROTONET code. ROTONET re-propagates the source sound field to a user-defined grid of ground locations which can include a large area enabling an estimation of noise patterns that were not directly measured. This method can avoid the limitations of the first-principles approach. This approach is being further developed as a research tool, Rotorcraft Noise Model (RNM) [2] to calculate and assess the noise propagated by civil tilt-rotor and to design low noise flight procedures [3].

A novel flight trajectory management model was introduced by Gopalan and Schmitz et al [4, 5] to help to explore flight profiles which minimize BVI noise radiation. The Quasi-Static Acoustic Mapping (Q-SAM) method was developed and used to relate helicopter performance and trajectory control to ground annoyance levels. The acoustic field on the hemisphere surface in Q-SAM model can be obtained from the numerical simulation or from direct steady-state trim acoustic measurement. However, it neglects the effect of vehicle acceleration on the radiated noise and ground reflection. Their studies for AH-1 helicopter show that the use of small deceleration at a steeper descent or X-force controls at a shallow descent can yield a quieter ground noise.

To develop and validate noise abatement flight procedures for rotorcraft, a joint U.S. industry/NASA/FAA flight test program was conducted during 1996 [6]. This program demonstrated noise reduction exceeding 6 dB could be achieved through noise abatement flight procedures. In order to satisfy the requirements of safe, low noise and effective helicopter flight operations, a very comprehensive flight test with a fully instrumented BO 105 helicopter was conducted on Cochstedt airport within the joint DLR/ONERA research concept [7]. The objective of the flight test was to generate a high quality aerodynamic and acoustic data base for the design of low noise flight procedures, particularly for descent flight and landing approach conditions. The test results will further serve for the validation of aerodynamic and acoustic prediction codes and for the verification of the equivalence of scaled model rotor wind tunnel and scale-1 flight test results. Furthermore, an internal DLR project, PAVE (Pilot Assistant in the Vicinity of Helipads) is initiated and currently conducted. The extensive flyover noise measurements in combination with pre-design low noise flight procedure will be carried out to help defining noise abatement procedure. The goal is to demonstrate a noise reduction of about 6dB by the end of the PAVE project. As a first step towards noise abatement flight procedure design, this report presents a DLR tool which is currently under development for rotorcraft noise ground footprint prediction using either purely theoretical computations or measured sound fields.

The approach adopted for the ground footprint prediction here bears strong similarity to the work of Wilson et al [1]. However, the required noise source value on the hemisphere surface in given space angle other than measured angle is directly interpolated using original angular coverage provided by the measured sound field. A two dimensional Lagrange interpolation schemes are used. In addition, the noise source description of the present method can base entirely on theoretical computations. For purely numerical simulation, only the MR and TR are simulated without the fuselage and the flight conditions restricted to subsonic incompressible flow.

The objective of this report is to present DLR tools used for rotorcraft noise ground footprints prediction. The major elements in the HEMISPHERE code are described. The interpolation scheme directly using original angular coverage provided by the measured sound field is introduced. The preliminary results of an ongoing

effort at DLR to simulate the aerodynamics and aeroacoustics of a helicopter main rotor (MR) and tail rotor (TR) configuration are presented. For the validation of the ground to hemisphere transformation implemented in HEMISPHERE code, the acoustic “ground” data taken from both pure numerical simulation results and flight test data are used. Finally, a simple flight procedure with combination of different segment of flight trajectories is tested to demonstrate the capability of DLR HEMISPHERE code

## GROUND FOOTPRINTS PREDICTION

The numerical technique for rotorcraft noise ground footprint prediction adopted in present paper can be divided into following steps. At first the detailed acoustic far-field or “Noise Source” on hemispherical surface beneath the aircraft is obtained using either purely theoretical computations based on first-principles or measured sound fields on a limited no. microphone or measured limited unsteady pressure data on the blade. Knowing the flight trajectory and the flight condition, the relevant hemisphere surface is then moved along the flight segment with the desired speed to obtain effective noise level on the ground. The structure of the DLR developed/used flyover noise prediction chain is shown in Fig.1.

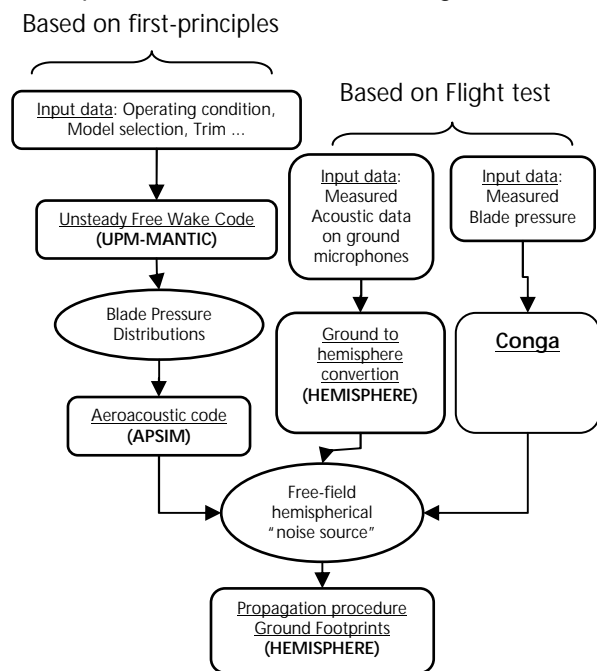


**Fig. 1** Structure of DLR developed/used flyover noise prediction chain

### Ground Footprints Estimation based on the first principle

As shown in Fig.1, in case of method based on first-principle required, the aerodynamic code, UPM-Mantic [8] for low speed BVI case (or FLOWer for high speed case) is used. The output will serve as input to a Ffowcs Williams-Hawkings (FW-H)-equation based code, APSIM [9,10] to define the acoustic pressure on a free-field hemispherical “noise source” surface beneath the aircraft. The hemispherical sound field is then provided to a flyover noise prediction code, HEMISPHERE [11,12] to fulfill footprints prediction.

### Ground Footprints Estimation Using Flight Test Data ( on ground microphone)

The most accurate method to generate acoustic footprints is a flight of the aircraft over a large number of ground microphones placed over the area of interest. Since operational aircraft under real flight conditions are employed, a comprehensive picture of the ground footprint is obtained for any flight condition of interest; but the large expense and data acquisition effort needed for this approach severely limit its applicability.

As an alternative for using a large number of ground microphones, the acoustic footprint can also be obtained indirectly using only data obtained from an array of microphones, based on condition that aircraft conducts a steady flight condition. Fig.2 gives such a microphone array composed of 11 microphones used in DLR “RONAP” Flight Test. In order to evaluate acoustic footprints using data from this microphone array, the two procedures are required. The first procedure as shown in Fig.3 is called in present report as Ground to Hemisphere Conversion (GHC). There are in general two steps in GHC. In the first step of GHC procedure, the acoustic directivity pattern or geometric relation represented in three dimension variables ( $R, \theta, \phi$ ) is calculated as a function of emission time for each microphone. The definition of ( $R, \theta, \phi$ ) is given in Fig.3. The knowledge of the propagation path (straight line from source to observer at current status), flight path, aircraft attitude and the speed of sound is utilized, based on the assumption that the microphone recording times are synchronized with the tracking time of the vehicle position. The second step is to transform the acoustic spectrum

acquired on the ground microphones into a free-field acoustic value by applying corrections on

1. Doppler effect on the received frequencies;
2. Spherical spreading or “inverse-distance” law and characteristic impedance effect;
3. Atmospheric absorption effect as a function of the distance traversed by the noise signal, the air temperature and relative humidity;
4. Ground reflection and attenuation effect.

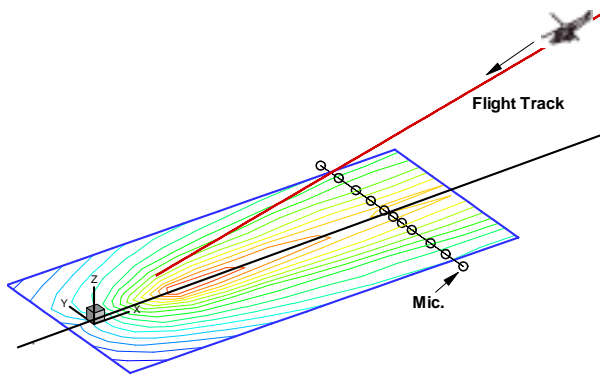


**Fig. 2** Perspective view of microphone array (composed of 11 microphones used in DLR “RONAP” Flight Test)

The results of the second step of GHC are a free-field hemispherical “noise source” surface beneath the aircraft at a constant radial distance. The free-field acoustic sound pressure data obtained is a function of frequency, polar directivity angle ( $\theta$ ) and azimuthal directivity angle ( $\phi$ ). Fig.4 is an example of such a directivity angular coverage constructed using measured flight trajectory in a 6 deg. descent flight. The plot demonstrates the projection of the hemisphere to a two dimensional plot. Each point on the plot correlates to each emission time and each column represents the data from same microphone. The directivity angles ( $\theta, \phi$ ) are in general irregularly distributed on the hemisphere.

The second procedure is a propagation procedure in order to extrapolate acoustic source from the acoustic hemisphere to the ground observer. In this procedure, the free field acoustic data on hemisphere surface is used to enable an estimation of acoustic footprints in a large area which may not directly measured, as shown in Fig.5. The direct

interpolation using original angular coverage provided by the measured sound field is used.

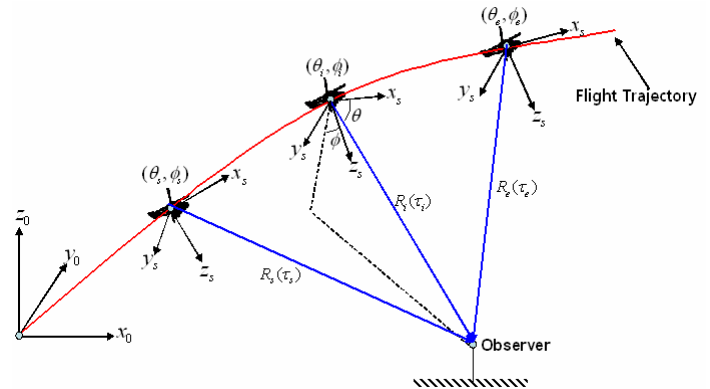


**Fig. 3** Geometric relation represented in three dimension variables ( $R, \theta, \phi$ ) as a function of emission time

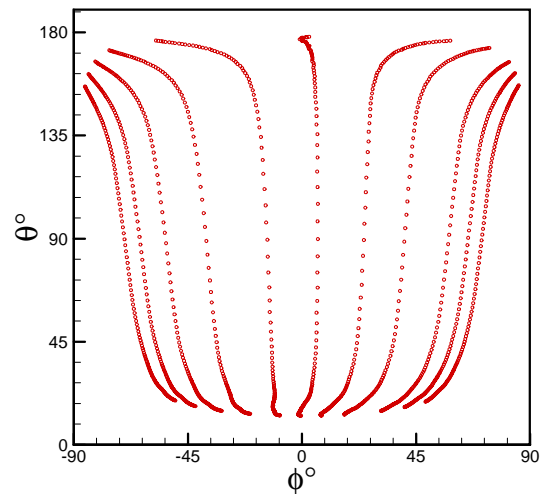


**Fig. 4** Directivity angle coverage on a hemisphere

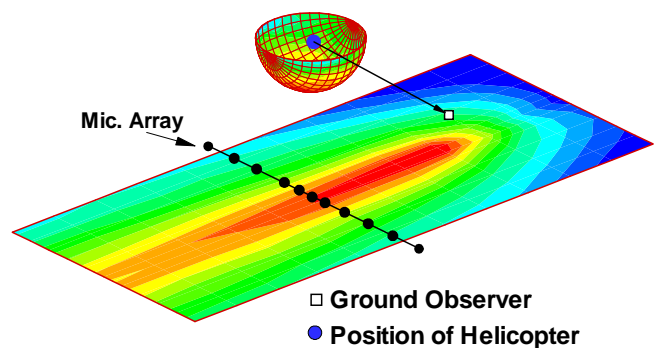


**Fig. 5** Acoustic footprints estimation from a known noise source on a hemisphere

This indirect method for ground footprints estimation using flight test data is implemented in DLR HEMISPHERE code. The detailed structure and functions of HEMISPHERE are given in [11, 12].

### Interpolation Scheme

In noise propagation procedure, the required noise source value at a space angle  $(\theta, \phi)$  which is other than measured one is required. The interpolations or extrapolations are necessary. In present paper, an interpolation directly using original angular coverage provided by GHC, shown in Fig.4 as an example, is used. The advantage is that the total angular coverage of measured sound field can be used.

The direct interpolation in present report involves several steps described in Fig. 6. First step is to find out 4 grid points in directivity angle domain  $(\phi, \theta)$  in which interpolation point is enclosed. Although presumably simple, the task is not at all trivial for the irregular angle distribution such as one in Fig.4. The task can be solved by computing the space angle of the periphery closed by 4 grid points. For interpolation point outside the periphery, the space angle is zero [13]. The second step is to transform from physical domain  $(\phi, \theta)$  (non-regular grid) into computation domain (equally spaced regular grid). The transformation is also made for the interpolation point (solid circle). The last step is to make interpolation in computation domain [14]. It is only necessary to know how to interpolate a point from a rectangular grid. Therefore, a two dimensional Lagrange interpolation scheme is used. The width of the interpolation stencil can be varied. In present paper, a 16 points scheme is used.

For a simple validation, a known test function  $f(\phi, \theta) = \sin(2.(\phi + \theta))$  is imposed on the grid points given in Fig.7, the value on the interpolation points were obtained using above interpolation schemes. Fig. 7 shows the interpolation points marked as open rectangular which will be interpolated from measured background grid marked as solid circles. The comparison of the contour plots are shown in Fig. 8. Fig. 8a shows the original test function associated with value on the solid circles, while Fig. 8b represents value on the open rectangular interpolated. The comparison of Fig.8b with area enclosed by a rectangle block

in Fig.8a shows interpolation scheme functions quite well.

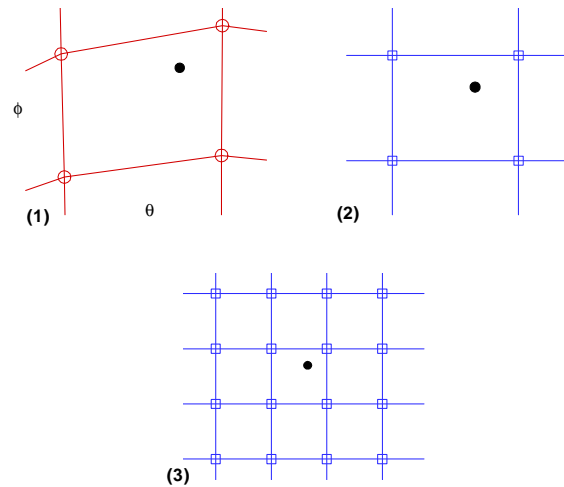


Fig. 6 Interpolation procedures

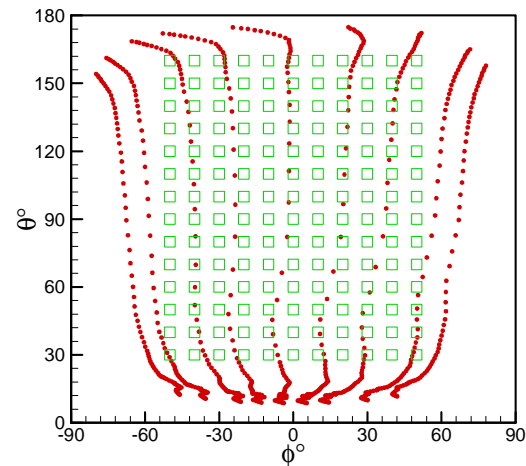
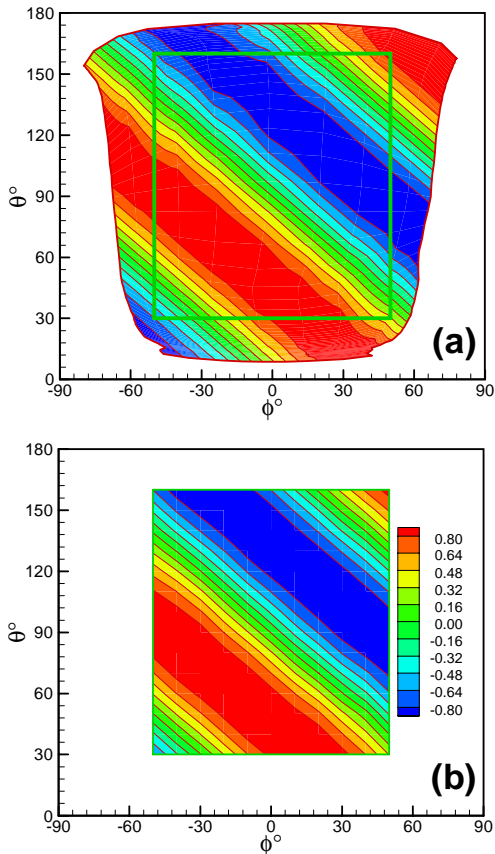


Fig. 7 Directivity angle coverage on a hemisphere including interpolation points

As mentioned in previous section, the interpolation scheme is implemented in HEMISPHERE code so that direct interpolation using original angular coverage provided by the measured sound field is possible.



**Fig. 8** Contour plots for a test function  
 (a) value on original grids;  
 (b) value on interpolation points

## HEMISPHERE CODE VALIDATION

### HEMISPHERE code validation using the first principle method

The noise ground footprints of a BO105 helicopter at two flight conditions are first simulated using first methodology- propagation procedure. These flight conditions are 6° descent flight in which main rotor BVI noise is dominated as well as 12° takeoff flight with tail rotor as dominant source of noise. The simulations are carried out in this study as a MR and TR configuration without the fuselage. The geometry, relative position, and the r.p.m ratios of the MR and TR numerical model match with the real aircraft. Flight speed was a constant 65 knots for both cases.

### 6° Descent Flight

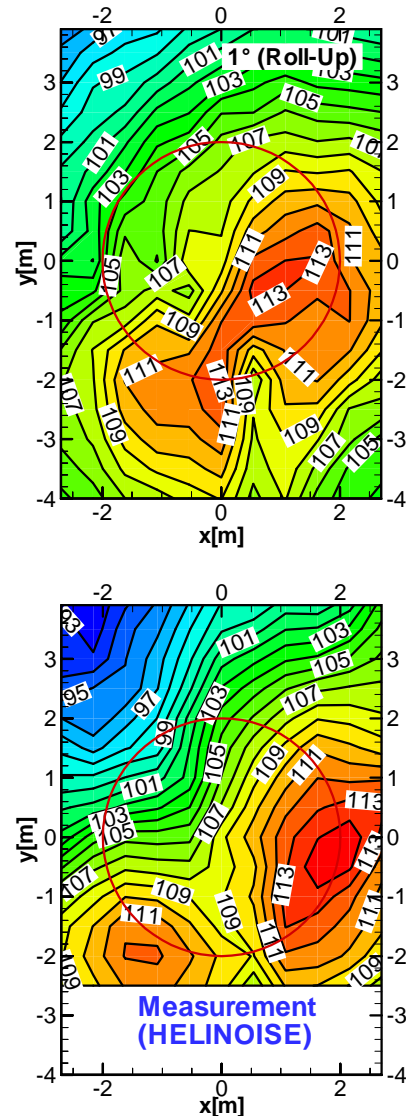


**Fig. 9** Comparison of the measured mid-frequency summary level noise contour and prediction obtained by using tip vortex roll-up model at 1° time step

In order to make comparison with wind tunnel test results, the combination of **UPM-Mantic** and **APSIM** code is first used to produce the mid-frequency summary level contour plots. The contour plots are taken from a near field plane situated 1.15 MR radii below the MR hub with a range of 2.7 x 4 MR radii. The comparison with measured mid-frequency summary level noise contour is given in Fig.9. The frequencies considered in this plot are from 6th to 40th harmonics of blade passage frequency, which is a

representative measure for BVI impulsive noise. The location of the MR disc is indicated by the red circle. The two maximum noise areas (hot spots) both in advancing and retreating side are captured in predicted noise contour. The maximum noise level is captured by the prediction as well.

To map the acoustic ground footprint, the acoustic pressure time histories radiated from both MR and TR are first summed in time domain and transformed into a narrow band spectrum on each reference points which are located on a hemisphere. The hemisphere is divided by 19x19 reference points in the longitudinal (-90° to 90°) and latitudinal (0-180°) direction. Each reference point is in 10 degrees apart. The radius of the hemisphere was chosen to be five times the radius of the BO105 MR. It is assumed that the noise propagation radially away from the hemisphere can be treated as “free” propagation and the non-linear effects neglected. The mid-frequency summary level noise contour plot as function of space angle on the hemisphere is shown in Fig. 10.

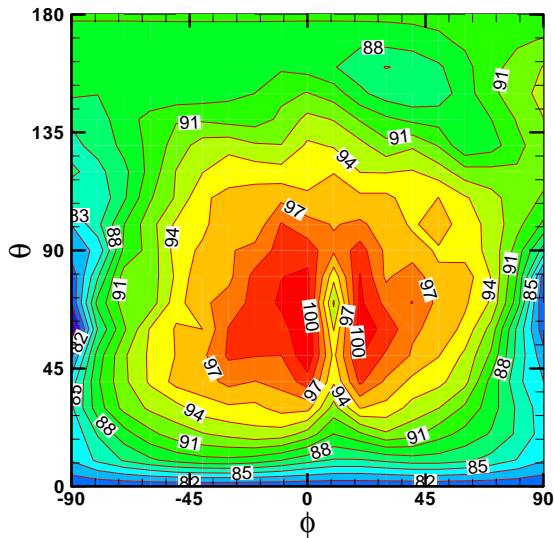


**Fig. 10** Mid-frequency summary level noise contour as function of space angle on the hemisphere

The flyover noise prediction procedure of HEMISPHERE code is used to propagate acoustic signal from hemisphere to the ground microphones. Fig.11 shows the characteristics of the resulting noise foot-prints in EPNL values. The flight trajectory is also given in the plot. The aircraft flies from right to left in the direction of the negative x-axis with a constant descent angle and flight speed. The over-flown area is 500 m wide and 1100 m

long. The noise computations stop when aircraft arrives at lowest point in the flight trajectory.

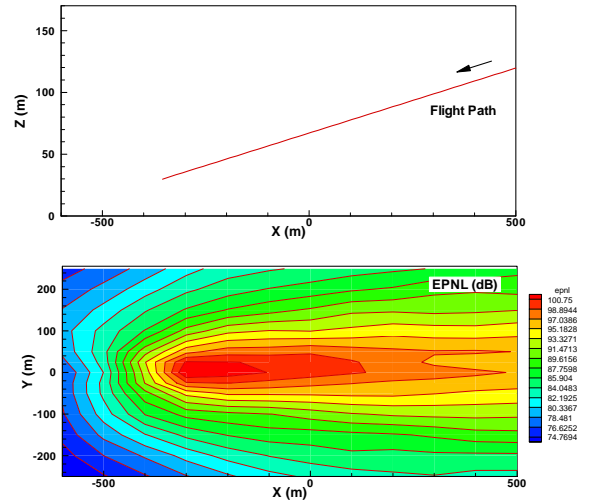


**Fig. 11** EPNL ground footprint and flight trajectory for a 6° descent flyover

In general, the maximum levels are located about the end point of the trajectory and decrease rapidly with increasing sideline distance and with increasing downrange distance. The contours decrease least rapidly along the flight path uprange of the end point, i.e., the area over which the aircraft actually flies. Up range along the flight path, the contour “tails” increase in both length and width with decreasing contour level.

### 12° Takeoff Flight

In contrast to the descent, the takeoff flight path is relatively short as most of the power is used now to gain height and forward motion is less. Accordingly the EPNL footprint contours exhibit a wider and rectangular shaped pattern as shown in Fig.12 for a 65 knots and 12° steep takeoff from right to left. The maximum EPNL values are here lower than in the case of descent, the reason being the rapid gain in height above the ground during the takeoff. During takeoff, the MR wake is pushed down and moves away from the MR disc so that interaction between MR blades and wake is reduced. The noise contribution from the TR would thus be dominant in this flight phase.

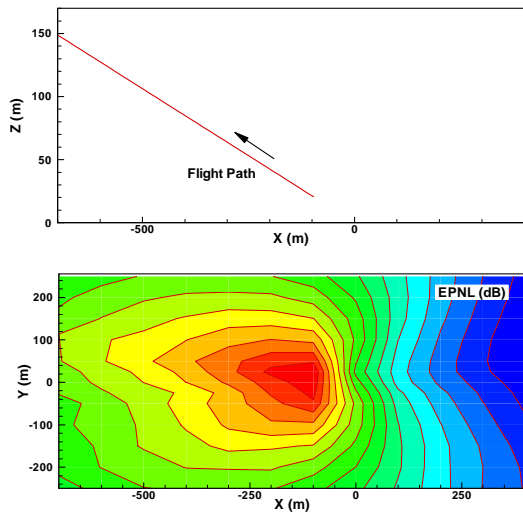


Fig. 12 EPNL ground footprint and flight trajectory for a 12° takeoff flight

### Validation on GHC Procedure using the first principle method

For the validation of the second methodology GHC implemented in HEMISPHERE code, the acoustic ground data taken from pure numerical simulation results are used. 6° descent case simulated in previous section are chosen for the validation. The ground microphones used in the ground to hemisphere transformation are distributed in an array which is perpendicular to the flight path, as shown in Fig.2.

The acoustic sound spectrum on the linear ground microphone array is first calculated using free field hemisphere data provided by APSIM code in combination with HEMISPHERE propagation procedure. The spectrum is a function of flyover time with a time step of 0.5 Sec. and 512 harmonics.

The acoustic spectra acquired on the ground microphones are then used as a input into HEMISPHERE to perform GHC-Procedure and create free field hemisphere surface. The propagation procedure in HEMISPHERE code is switched on for a footprint on a user-defined grid of observer locations. Fig.13 (b) gives the EPNL footprints obtained after GHC procedure and its comparison with direct simulation. As can be seen, the results obtained through GHC procedure closely match the results from direct prediction.

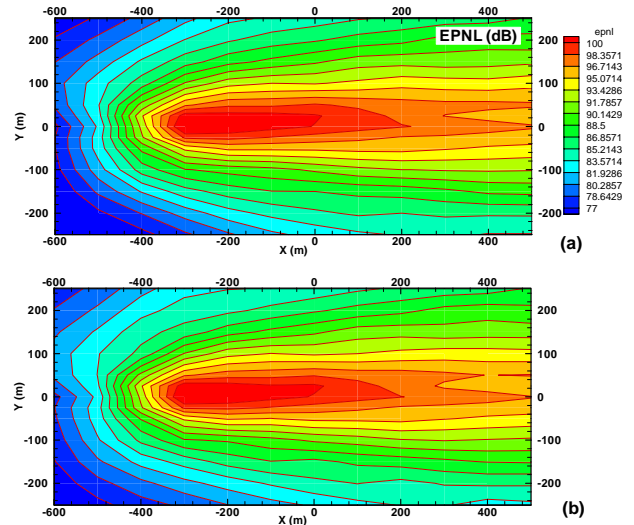


Fig. 13 EPNL ground footprint obtained after reverse procedure (b) and its comparison with direct simulation (a)

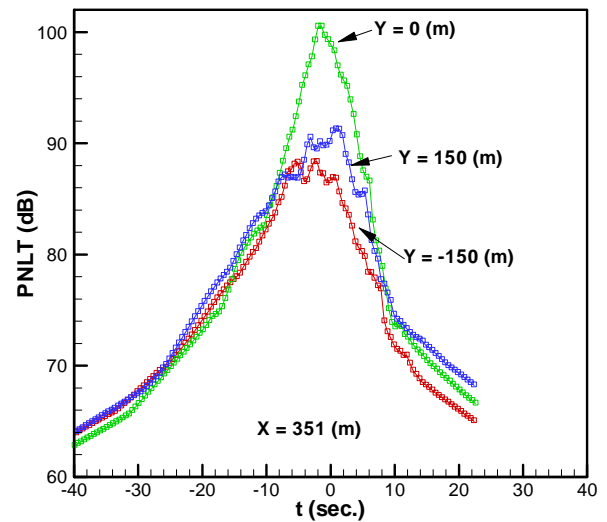


Fig. 14 Comparisons of PNLT values at 3 observer locations such as x=351(m), y=-150, 0.0, 150 (m); Symbols represent results obtained directly

Another validation that can be made involves looking at time history of PNLT. Fig.14 demonstrates comparisons of PNLT values at 3 observer locations such as x=-150, 0.0, 150 (m). Symbols represent original PNLT values obtained directly and lines represent the values obtained after the reverse propagation procedure. The zero on the time axis indicates the time at which the aircraft is closest to the observers. The results

compare quite well for the entire flyover. Fig.15 presents the EPNL as a function of the sideline distance and its comparisons with direct simulation. In general, the greatest variation occurs directly under the flight track and decays gradually with increasing sideline distance, but a slower decaying rate is observed in advancing side microphones (positive y value). The comparison shows again perfect agreement.

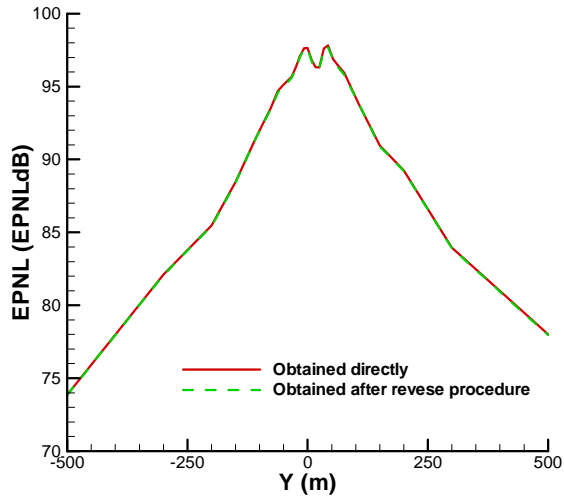


Fig. 15 EPNL as a function of the sideline distance and its comparisons with direct simulation.

### HEMISPHERE code validation using flight test data

The code validation using pure numerical simulation results were described in previous section. In this section, the code is validated using real flight test data from DLR "RONAP" Flight Test. Two flight conditions are employed in the validation. These flight conditions are 6° and 9° descent flight at a nominal speed of 33m/sec, respectively. The ground microphones used in the flight test are shown in Fig.2.

The procedure GHC described in the previous section is first used to generate free field lower hemisphere sound field for each flight condition. The measured acoustic spectrum on the ground microphones is used as input. For the validation purpose, output is chosen on the locations where ground measurement was conducted in the flight test.

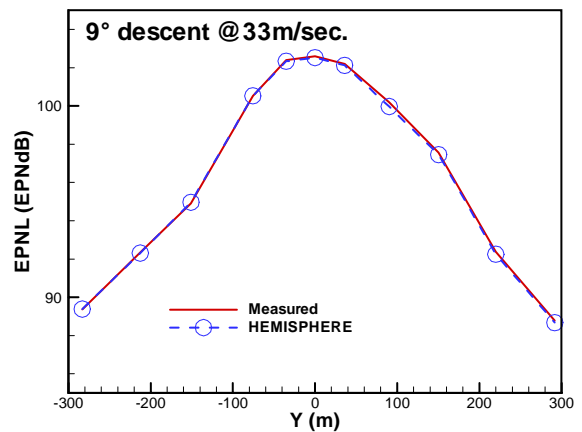
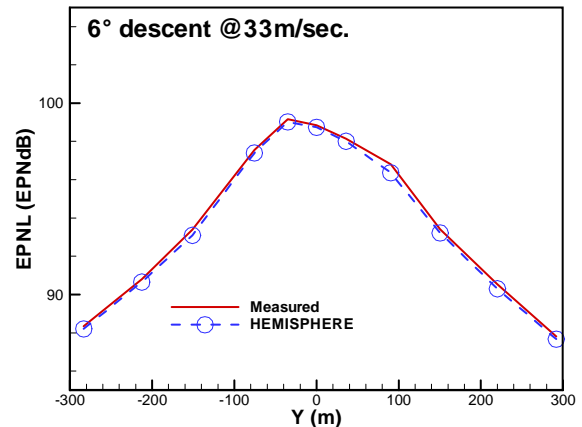


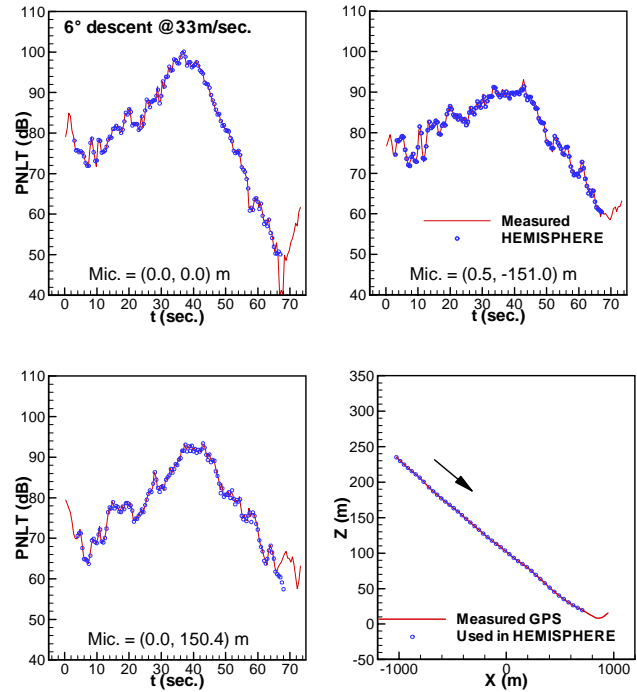
Fig. 16 EPNL as a function of the sideline distance and its comparisons with measurement

Fig.16 presents the EPNL as a function of the sideline distance and its comparisons with flight test data for both 6° and 9° descent cases. EPNL values are calculated based on a 10-dB down criteria from the PNL time series data. It should be mentioned that due to the effects of wind the aerodynamic slope and geometric slope measured from GPS data are different. The slope given in the plot is a geometric slope relative to the ground. The preliminary velocity correction given in [7] shows that the aerodynamic slope is around 4° for the descent flight in 6° geometric slope. The detailed 7-hole probe calibration is still under way. Therefore, the descent angle is all reference to the geometric slope angle if it is not specifically mentioned in following sections.

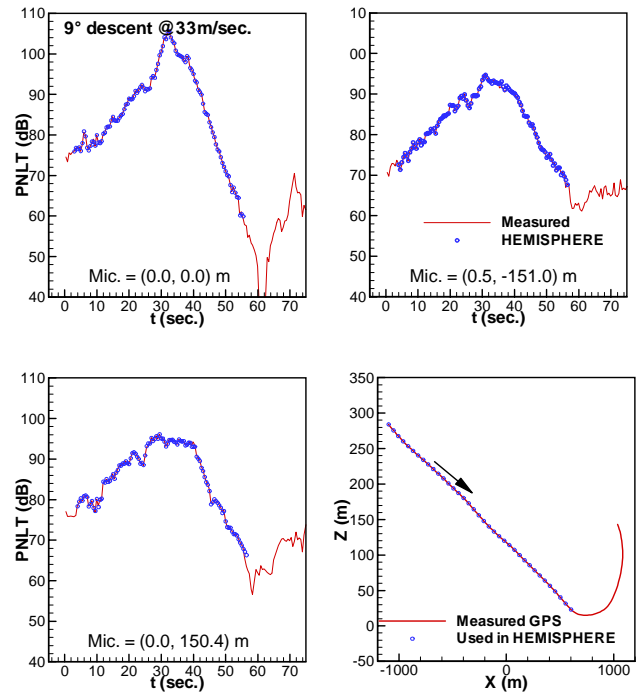
In general, excellent agreement is shown between the measured and predicted EPNL for all the microphone positions. The 6° approach appears to be less noisy compared to the 9° approach. The maximum EPNL levels occur directly on the centerline for 9° descent case and shifts somewhat towards the retreating side for 6° descent. For both cases, the levels fall off quickly with increasing sideline distance, but a slower decaying rate is observed in advancing side microphones (positive y value).

Another validation that can be made involves looking at time history of PNL. Fig.17 demonstrates comparisons of PNL values with flight test data at several observer locations. The two-dimensional flight path is also given in the plot. GPS data indicate some maneuvering flight parts are included in the measurements, but only data corresponding to the steady flight period (marked as blue circle in GPS plot) are employed in the HEMISPHERE. The time axis indicates the reception time in the plot. The measured PNL time history presented in the Fig.8 corresponds to the whole measured period. The results compare quite well for the entire steady flyover period.

It has to be mentioned that in real measurement the acoustic spectrum is given according to an equal frequency bin width defined by the window duration employed by FFT algorithm. This frequency bin width should be small enough to resolve relevant spectral features or all the harmonics. In addition, direct interpolation by fully using measured directivity angle coverage on a hemisphere is again recommended .



(a) PNL time history and GPS value for 6° descent flight



(b) PNL time history and GPS value for 9° descent flight

Fig. 17 Comparisons of PNL time histories with flight test data

## NOISE ABATEMENT FLIGHT PROCEDURE

Two simple flight procedure with combination of different segment of flight trajectories and speeds are tested to demonstrate the capability of DLR Hemisphere code. The flight test data are used.

### Multi-descent angle with constant flight speed

During a nominal approach to a landing, a helicopter pilot typically executes a small number of constant glide-slope segments before the final stages of flare and touch down. In order to reduce flyover noise in 9° descent, two multi-segmented noise abatement approach profiles as shown in Fig.18 are conducted for a preliminary noise abatement flight procedures design test. Multi-segmented approach profiles are composed of several more segments, each defined by a set of parameters that remain constant through out that segment. The defining parameters in general can be flight path angle, flight speed and deceleration, etc, but only flight path angle is used as the defining parameter for each segment in present report. The initial points in the flight trajectory are closer to the initial point of the 9° approach. The end points of the flight trajectory are same.

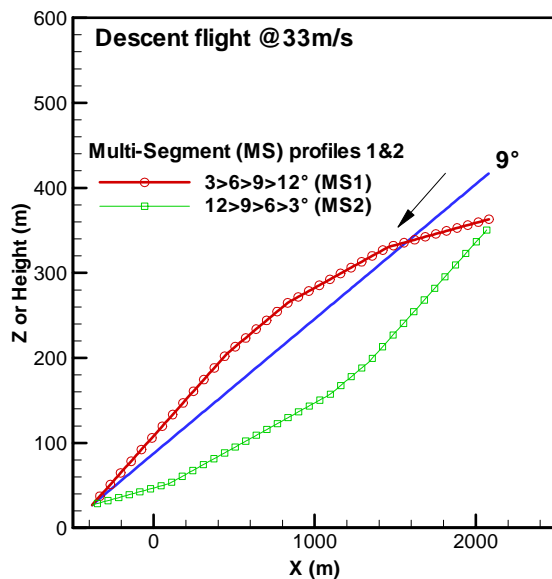


**Fig. 18** Description of two Multi-segmented approach profiles

Each profile given in Fig.18 consists of 4 flight segments, each defined by the flight path angle. The flight path angle changes from one segment to

next without considering transition between them. The figure shows that for Multi-segment 2 (MS2) the helicopter starts to decline in a higher descent angle or flight path angle (12°) segment and decreases stepwise to 9°, 6° and 3° segment, and helicopter finally approaches to the end point with 3° descent angle. The length of each segment is proportional to the overall flight time. Table 1 gives percentage of the flight time for each segment in proportion to the overall flight time. It shows that less flight time is given for 9° (maximum BVI case) in order to minimize contribution of 9° descent segment. In Multi-segment 1 (MS1) flight profile, the helicopter starts to fly from lowest descent angle 3° segment and increases stepwise to 6°, 9° and 12° segment, and helicopter finally approaches to the end point with 12° descent angle. Compared with MS2, MS1 profile creates large altitude and source-receiver distance.

**Table 1** Percentage of the flight time for each segment

	12°	9°	6°	3°
MS1	35%	15%	25%	25%
MS2	30%	10%	40%	20%

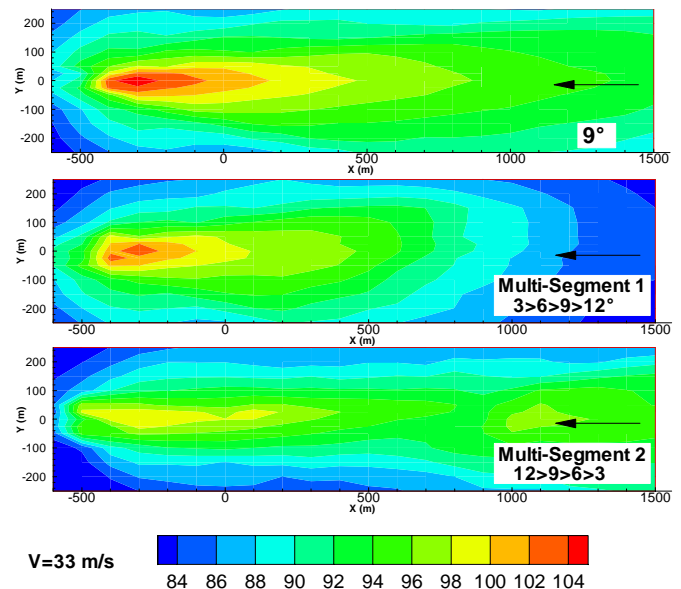


**Fig. 19** EPNL ground footprint at multi-segment flight profiles for a constant flight speed

To map the acoustic ground footprint, hemisphere selection may be necessary when change of flight condition e.g. flight path angle occurs during the

flight. At present HEMISPHERE code, the time points when flight condition changes are specified and given in input data. The condition required to chose different hemisphere data are according to the specified time points. There are no limits on number of hemisphere.

Fig. 19 shows the characteristics of the resulting noise footprints for the two multi-segmented approach profiles. For comparison with high BVI case, the footprints plot for 9° descent case is again plotted.

Compared with footprints of 9° approach, Figure 19 clearly illustrates that the multi-segment noise abatement procedures are effective and provide clear evidence that approach noise reductions are achievable. The footprint exhibit significant noise reductions for multi-segement 1 at area up-range of 1000m and for multi-segement 2 at area up- and down-range around end point. MS2 approach is quieter around landing point because the aircraft is on the quiter 3° glide slope but louder at up-range from x=1000m due to 9° BVI segment.

To provide a more quantitative assessment of the EPNL differences for the different approach profiles, Figure 20 presents the EPNLs as a function of the sideline distance for a number of slices across the noise footprint located -400, 0, 500 and 1000 m, respectively.

For the slice at 1000m, Figure 20 shows that on the centerline, the multi-segment 2 approach has the highest EPNL while the the multi-segment 1 approach has the lowest EPNL and the difference between MS1 and MS2 is about 10 EPNdB. However, for the sideline locations the 9° approach generally has the highest EPNL.

For the slice at 500 and 0 m, Figure 20 shows that the the multi-segment 1&2 approach has the lower EPNL for all sideline locations. At -400 slice position, Multi-segment 1 approach has higher EPNL for all the sideline position at retreating side (negative y) while Multi-segment 2 approach keeps lowest EPNL level. EPNL drops rapidly for the sideline position up-range of 100m. for both Multi-segment approaches.

Figure 21 shows the EPNL averaged over the contour area given in Fig.17. This figure shows that noise reduction can be obtained by using both multi-segment approaches. Averaged EPNL for the multi-segment 2 approach is almost 2.5 EPNdB lower than the 9° approach.

It has to be mentioned that transient maneuvers effects from one flight path angle to the other are not considered. The characteristics of flyover noise may be different when these effects are included.

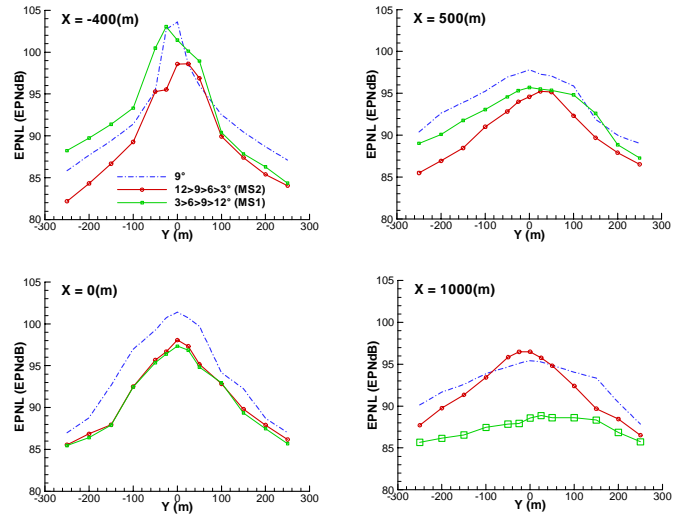


Fig. 20 EPNL as a function of the sideline distance for a number of slices across the noise footprint

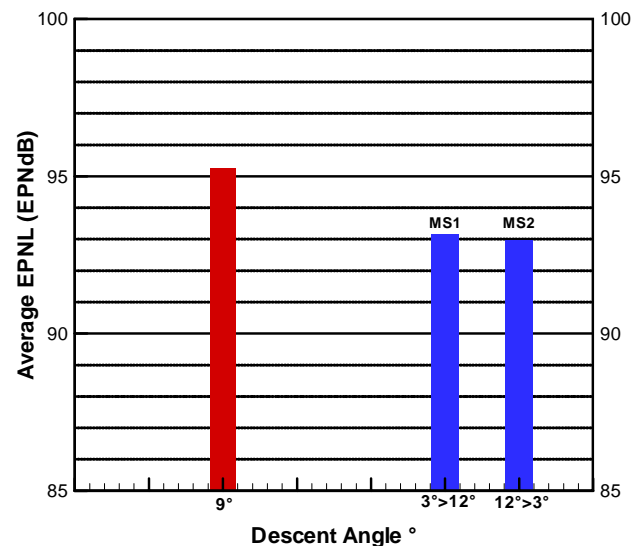


Fig. 21 Averged EPNL for the different approach

**Multi-flight speed with constant descent angle**

A multi-flight speed descent flight procedure with constant descent angle is tested as a final example.

9° descent flight is again chosen as baseline case. The flight speeds are varied from 33m/s to 15m/s in a multi-segment decelerated manner. The portion of each flight speed is given in Fig. 22 and table 2. The transition from one speed to the other is in stepwise. The DLR flight test data are again used.

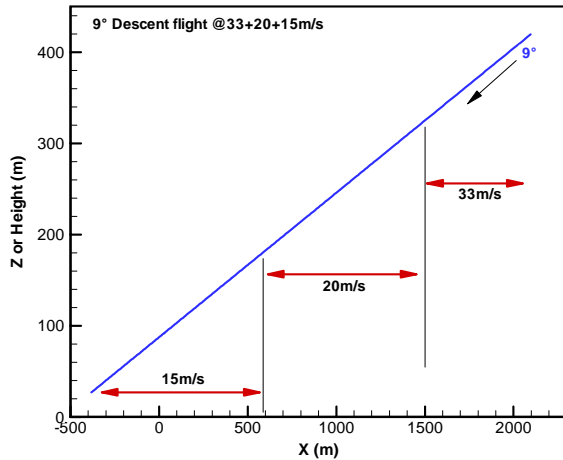


Fig. 22 Description of Multi-Flight speed approach with constant descent angle

Table 2 Percentage of the flight time for each flight speed

	33m/s	20m/s	15m/s
MFS	15%	35%	50%

Fig. 23 shows the characteristics of the resulting noise footprints for the multi-flight speed (MFS) approach. The footprints plot for 9° descent case at constant flight speed is also given in the plot for the comparison. Fig. 24 demonstrates the averaged EPNL value and its comparison with results obtained by MS 1&2. The benefit of noise reduction with MFS procedure is very close to MS 1&2. These results further indicate that noise abatement flight procedure can be achieved.

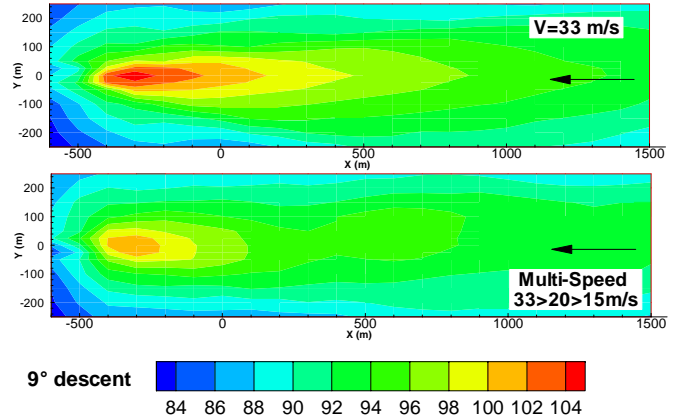


Fig. 23 EPNL ground footprint for a multi-flight speed decelerating case

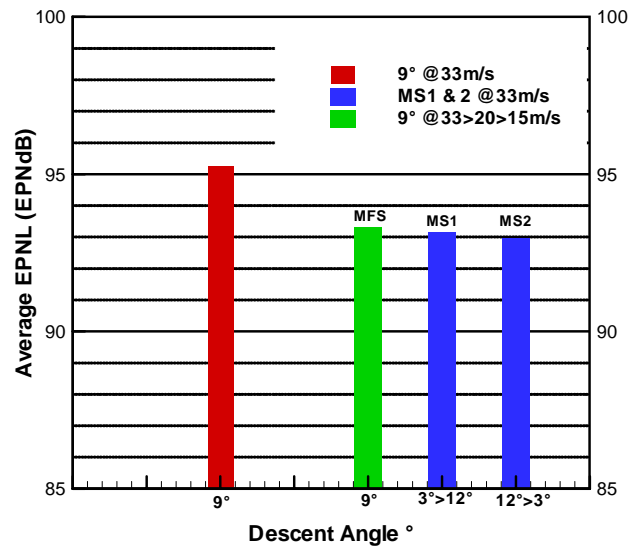


Fig. 24 Averaged EPNL for the different flight procedure

## SUMMARY

This paper describes the methods used in DLR for rotorcraft noise ground footprints prediction. The validations of the methods are based on both the purely numerical simulation and real flight test. The numerical model employed simulates only the MR and TR without the fuselage and constant speed flight. The flight test data are taken from the RONAP flight test conducted on Cochstedt airport, Germany in 2001. The interpolation scheme directly using original angular coverage provided by the measured sound field is introduced and validated

using an analytical solution. Two multi-segmented approach profiles consisting of a series of constant flight path angle segments and one multi-flight speed decelerating case are tested and flyover noise reductions are observed.

## REFERENCES

- [1] M.R. Wilson, A.W. Mueller, and C.K. Rutledge, "A New Technique For Estimating Ground Footprint Acoustics For Rotorcraft Using Measured Sound Fields", Paper presented at the American Helicopter Society Vertical Lift Aircraft Design Conference, San Francisco, California, USA, Jan. 18-20, 1995
- [2] M.J. Lucas and M.A. Marcolini, "Rotorcraft Noise Model", Paper presented at the American Helicopter Society Technical Specialists' Meeting for Rotorcraft Acoustics and Aerodynamics, Williamsburg, VA, Oc.. 28-30, 1997
- [3] D. Conner, J. Page, "A Tool for Low Noise Procedures Design and Community Noise Impact Assessment: The Rotorcraft Noise Model (RNM)", Paper presented at Heli Japan, Tochigi, Japan, Nov. 11-13, 2002
- [4] G. Gopalan, F.H. Schmitz, and Wel-C. Sim, "Flight Path Management and Control Methodology to Reduce Helicopter Blade-Vortex Interaction (BVI) Noise", Paper presented at the American Helicopter Society Vertical Lift Aircraft Design Conference, San Francisco, CA, Jan., 2000
- [5] F.H. Schmitz, G.G. Ben, and Wel-C. Sim, "Flight Trajectory Management to Reduce Helicopter Blade-Vortex Interaction (BVI) Noise with Head/Tailwind Effects", Presented at the 26th European Rotorcraft Forum, The Hague, The Netherlands, September 26-29, 2000
- [6] E.W. Jacobs R.D. Prillwitz, R.T.N. Chen, W.S. Hindson, and O.L.S. Maria, "The development and flight test demonstration of noise abatement approach procedures for the Sikorsky S-76", Paper presented at the American Helicopter Society Technical Specialists' Meeting for Rotorcraft Acoustics and Aerodynamics, Williamsburg, VA, Oct.. 28-30, 1997
- [7] P. Spiegel, H. Buchholz and W. Spletstoesser, "The "RONAP" Aeroacoustic Flight Tests with a Highly Instrumented BO105 Helicopter", Paper presented at the American Helicopter Society 59<sup>th</sup> Annual Forum, Phoenix, Arizona, May 6-8, 2003
- [8] J. Yin, S. Ahmed, "Helicopter main-rotor/tail-rotor interaction", Journal of the American helicopter society, Vol. 45, No. 4, pp293-302, October 2000.
- [9] M. Kuntz, "Aeroacoustic Program System APSIM, User Handbook, Release 5.2", April, 2000.
- [10] J. Yin and J. Delfs, "Improvement of DLR Rotor Aeroacoustic Code (APSIM) and its Validation with Analytic Solution", Paper-No. 2, 29th European Rotorcraft Forum 16 - 18 Sep. 2003 Friedrichshafen, Germany
- [11] J. Yin, "TOWARDS NOISE ABATEMENT FLIGHT PROCEDURE DESIGN: DLR Rotorcraft Noise Ground Footprints Model and its Validation", DLR IB 129-2004/14, April, 2004.
- [12] J. Yin, "Rotorcraft Noise Ground Footprints Estimation and Preliminary Lower Noise Flight procedure design Using DLR Flight Test Data", DLR IB 129-2004/19, July 2004.
- [13] J. Delfs, "An overlapping grid technique for the use of high resolution schemes of computational aeroacoustics at complex geometries", AIAA Paper 2001-2199, 7th AIAA/CEAS Aeroacoustics Conference 2001.
- [14] J. Yin; J. Delfs, "Sound generation from gust-airfoil interaction using CAA-Chimera method", AIAA Paper No. 2001-2136.